

Effect of shear stresses on adenovirus activity and aggregation during atomization to produce thermally stable vaccines by spray drying

Blair A. Morgan^a, Myla Manser^a, Mangalakumari Jeyanathan^b, Zhou Xing^b, Emily D.

Cranston^{a,c,d}, Michael R. Thompson^{a,*}

^a Department of Chemical Engineering, McMaster University, Hamilton, Ontario, L8S 4L7, Canada

^b McMaster Immunology Research Centre and Department of Pathology and Molecular Medicine, McMaster University, Hamilton, Ontario, L8S 4L7, Canada

^c Department of Wood Science, University of British Columbia, 2424 Main Mall, Vancouver, BC, V6T 1Z4, Canada

^d Department of Chemical and Biological Engineering, University of British Columbia, 2360 East Mall, Vancouver, BC, V6T 1Z3, Canada

*Corresponding author: Michael Thompson, mthomps@mcmaster.ca

Abstract

Considering the substantive potential benefits of thermally stable dry powder vaccines to public health, causes for inactivation of their sensitive viral vectors during preparation require intensive study. The focus of this work was atomization of suspensions containing encapsulating excipients and a human type 5 adenovirus, involving a detailed investigation of shear stresses in the nozzle of a spray dryer. Samples were sprayed at 25 °C into falcon tubes and immediately evaluated for viral activity by *in vitro* testing, minimizing the confounding of thermal effects on the deactivation of the virus. Despite expectations of only virus deactivation with ever-increasing shear stresses in the spray nozzle, some conditions were found to show better activity than the positive control, leading to investigations of viral aggregation. It was found that the adenovirus experienced minor aggregation when mixed with the excipient solutions, which was reversed by subjecting samples to moderate shear conditions in the spray nozzle. At very high shear rates, activity diminished again due to damage to the viral capsid fibers, which also led to the production of new aggregates after atomization. Despite these findings, activity losses caused by shear were small compared to the overall spray drying process loss. However, formulation composition, solution viscosity and process conditions should be considered carefully for medicinal optimization due to their impact on aggregation. This is the first known report comparing shear, aggregation, and biologic activity loss during the atomization step of spray drying thermally stable viral vaccines.

Keywords

Shear stress, aggregation, spray drying, particle sizing, process stresses, deactivation

1. Introduction

The immobilization of viruses and viral vectors such as adenovirus, herpes simplex virus, measles virus, and Newcastle disease virus in excipients like mono-, di- and poly-saccharides by spray drying has proven to be promising in preparing vaccines with high thermal stability, minimizing the necessity for adhering to cold chain protocols in maintaining long term efficacy.¹⁻⁴ Risk mitigation in spray drying for vaccine manufacture requires an analysis of its unit operations including pumping, atomization, drying, and collection, and evaluating their detrimental effects on the viral vector being stabilized.⁵ These unit operations expose any viral vector to thermophysical stresses, growth of the air-liquid interface, and desiccation, all of which are potentially damaging to these sensitive biologics.^{5,6} There are many studies in the literature on damage to enzymes, proteins, and bacteria during spray drying but no guidance on the harmful impact to viruses or viral vectors, which are more sensitive functionally to structural changes.⁷⁻⁹

The disclosed research is part of a series of studies examining the elementary factors of spray drying influencing the potency of thermally stable vaccines based on adenoviral vectors. Through optimization studies, viral activity was recognized to be dependent on system temperature and spray gas flow rate (and therefore shear) during spray drying, though the scope of prior work did not analyze the factors in detail or attempt to decouple interacting parameters.^{3,10} Subsequently, thermal stresses were examined with the same adenovirus in studies of droplet drying with an acoustic levitator, finding that moderately heated air (30 - 55°C) could actually decrease activity losses by causing faster immobilization of the viral vector in a solidified matrix of mixed saccharides.¹¹

One major difference between spray drying and acoustic levitation is atomization prior to droplet drying in the former case. Common to pharmaceutical spray drying, atomization involves two impinging fluids, compressed gas and a liquid suspension (containing the stabilizing excipients and the viral vector in our case) to produce a fine dispersion of droplets.¹² This subjects the liquid to large shear stresses that are proportional to the feed rates of these two fluid streams and the design of the nozzle.⁹ However, looking for specific atomization examples within the spray drying literature shows that little is known about the damaging effects of shear on biologics, with only two reliable cases in which both found the effect to be insignificant.^{13,14} In fact, no examples exist for viruses other than what can be indirectly implied from spray drying optimization studies.^{3,10} The most comprehensive previous study on shear damage of a biologic related to spray drying, found that up to 93% of bacterial death occurring during spray drying of *Lactococcus lactis* and the damage was attributed to shear stresses during atomization by the spray nozzle.⁹ Considering bacteria are commonly an order of magnitude larger than adenoviruses making them more prone to high shear stresses based on contact area, and the differences in structure and mechanical properties of gram-positive bacteria versus viruses, these results have little applicability to the present work and their study provided limited information by only investigating three shear rates.^{15,16}

The recognized effects of shear on biologics are conformational changes to enzymes, proteins, and components of the viral capsid, as well as disrupting the RNA/DNA structure of biologics such as viruses and bacteria.^{7,17} Maa and Hsu investigated the effects of shear, or shear combined with increased interfacial area, on the activity of two model proteins using either a concentric-cylinder shear device or a rotor/stator homogenizer in the presence of air.^{7,18} They concluded that denaturation resulted from shear damage and changes to the protein conformation

increased due to growth of the air-liquid interface. More specifically for viruses, virus-like particles, and viral surrogates, a small number of studies on shear damage are found in the literature (though not directed to spray drying). Michalsky et al. considered the effect of shear stresses attributed to stirring and pumping but did not observe any change in infectivity of a recombinant baculovirus of *Autographa californica* M nucleopolyhedrovirus.¹⁹ The shear rates in that case were far too low to be comparable to the two-fluid nozzle of a spray dryer, making it difficult to interpret its relevance to the current work. D'Souza et al. used high-pressure homogenization to investigate pressure, shear stresses, and temperature as parameters affecting human enteric virus surrogates, and found up to 3 log loss was obtained, although the effects were not differentiated in their analysis of causes.²⁰

The objective of the current work was to conduct a detailed investigation on the effects of shear stresses (under 15 different shear conditions) in a spray dryer nozzle on a frequently utilized vaccine platform, the human type 5 adenovirus, dispersed in a solution of mono- and poly-saccharides. Since spray drying inherently produces an increase in the air-liquid interface, the effect of shear will be confounded with this contributing effect in the study. *In vitro* activity testing was done before and after shearing. We also investigated the effect that shearing has on adenovirus aggregation, and how that may be related to changes in activity due to shear stress.

2. Materials and Methods

2.1. Chemicals and adenoviral vector

Excipients D-mannitol and dextran (M_r 40,000 kDa) were purchased as USP grades from Millipore-Sigma (Ontario, Canada). Purified water was produced using a Barnstead GenPure Pro water purification system from ThermoFisher Scientific (Waltham, MA) with a resistivity of 18.2 M Ω cm. Life Technologies protocols were used to prepare cell media in-house from α -

minimum essential medium (α -MEM) supplemented with 10% fetal bovine serum and 1% streptomycin/penicillin (Invitrogen, Ontario, Canada). A recombinant replication deficient human serotype 5 adenovirus expressing green fluorescent protein (AdHu5GFP) was produced in-house at the vector facility of the McMaster University Immunology Research Center as described previously.^{21,22} The stock viral vector suspension consisted of phosphate buffered saline (PBS) with 10% by volume glycerol. Each milliliter of viral stock contains 4.3×10^{12} viral particles, and 5.1×10^{10} plaque forming units (pfu). A deactivated AdHu5GFP sample was prepared by exposing 20 μ L of stock adenovirus suspension to UV light for 45 minutes in a biosafety cabinet. *In vivo* activity via flow cytometry (as described in Section 2.5) was used to confirm that the virus was deactivated by comparing the GFP expression of the deactivated virus sample to a negative control with no virus.

2.2. Atomization experiments

Trial solutions for the study contained 4% or 8% by weight of an excipient blend at a ratio of 3:1 mannitol:dextran, which was previously found to be highly effective for thermal stabilization of the (non-enveloped) AdHu5GFP viral vector.^{23,24} The viral vector stock suspension (10 μ L) was added to 10 mL of excipient solution, yielding a viral concentration of 5.1×10^7 pfu. To ensure homogeneity of the tested mixtures, the stock virus suspension was gently mixed in its vial by repeated inversion by hand before being added to the excipient solution. Once combined, the total excipient and virus suspension was taken up into the pipette tip (10 μ L) and re-ejected into the vial and this gentle mixing by pipette was repeated five times combined with inverting the vial five times. Sources of added shear stress, such as vortex mixing, were avoided during preparation of the test suspensions. In order to control the shear stresses of atomization under investigation, a B-290 Mini Spray Dryer (Büchi, Switzerland) was

used.^{4,10,11} The spray nozzle (0.7 mm diameter) was operated at room temperature to minimize thermal stresses on the viral vector, and atomized samples were collected directly into 50 mL Falcon tubes while still in liquid form. The characteristic shear rate at the nozzle tip was controlled by adjusting the spray gas feed rate between 282.9 and 1743.7 L/h, and setting the liquid feed rate to 188.5, 290.0, or 440.0 mL/h.

For all experiments that did not require viral activity testing, AdHu5GFP was not included in the formulation to minimize vector usage and meet biosafety requirements (the active virus is classified as biosafety level II); since the compositional fraction of the viral was very small (approximately 0.1 wt%) in the formulation, there would be no observable rheological difference in the solution by its absence. The reported data were collected from 3-4 repeated trials, conducted separately by two researchers over a span of several months. Positive controls constituted either a 10 mL 4% or 8% excipient solution with 10 μ L viral vector stock suspension added, without any shear applied, hereafter referred to as the “zero shear” samples. The test suspensions used for the “zero shear” samples were prepared in the same manner as those for the sheared samples.

2.3. Excipient solution viscosity

Dynamic viscosities of the excipient blend solutions, at 4% and 8%, were measured using a Discovery Hybrid Rheometer (TA Instruments; New Castle, DE) with a Peltier plate using a 40 mm cone geometry. Testing was done at a controlled temperature of 25°C by a frequency sweep from 0.1 to 5000 rad/s using approximately 0.5 mL of solution.

2.4. Viral aggregation measurements

Viral aggregation was measured using a qViro-X nanoparticle counter (Izon Science; Christchurch, New Zealand) with a NP150 thermoplastic polyurethane membrane with a single

nanopore. The analysis range of the NP150 covers particle sizes in the range of 70 to 420 nm (Izon Science; Christchurch, New Zealand). Sheared samples composed of virus and excipient, as well as the “zero shear” samples, were diluted by a factor of five in electrolyte buffer (10 mM HEPES, 150 mM NaCl and 4% by weight sucrose) to increase conductivity within the range required for the qViro-X instrument before testing. An adenovirus control was composed of 10 μ L of the viral vector stock suspension diluted by adding 990 μ L of electrolyte buffer, without excipients, in order to measure the aggregation of the stock virus suspension. It was necessary to dilute the stock virus suspension further than other samples in order to meet the recommended particle concentration for the qViro-X instrument (1×10^{10} particles/mL). All experiments were run with a voltage of 0.46 V applied across the pore. A pressure of 0.6 kPa was applied to the fluid cell using the instrument’s variable pressure module to increase the rate of particles passing through the pore. Samples were measured until either 500 events had been recorded or 10 min had elapsed, limited by the qViro-X control software. The relationship between blockade event magnitude and particle size was calibrated using CPC100 qNano carboxylated polystyrene calibration beads (Izon Science; Christchurch, New Zealand) with a mean particle size of 115 nm.

2.5. *In vitro* activity testing

In order to minimize potential adenovirus activity loss during storage at room temperature, sheared samples were stored on ice and tested on the same day they were produced. 100 μ L of a collected sheared sample (excipient and virus) was mixed with 900 μ L of culture media. A549 lung epithelial cells were cultured for five to seven days, until 80 – 90% confluent, then plated into a 96 well flat bottom plate at a concentration of approximately 4×10^4 cells per well. Each well was then incubated with 100 μ L of the sample/media mixture overnight, after which point the cells were prepared for flow cytometry. Media was aspirated from the wells and

each well was rinsed with 100 μ L of PBS. Cells were then trypsinized, and each well was pipetted into a plastic 5 mL round-bottom flow cytometry tube (Corning; Corning, NY) before being centrifuged at 1400 rpm for 5 minutes. The supernatant was discarded and 1 mL of PBS containing 2 mM ethylenediaminetetraacetic acid (EDTA) was added to prevent clumping. The cells were again centrifuged at 1400 rpm for five minutes, the supernatant was discarded, and 1 mL of 1% paraformaldehyde (PFA) was added to each tube to fix the cells. Finally, the cells were centrifuged at 1800 rpm for five minutes, the supernatant discarded, and 200 μ L of FACS buffer (0.5% w/v BSA in PBS) was added.

The prepared cells were processed according to the Miltenyi Biotec instructions for flow cytometry and run on a MACSQuant Analyzer 10 (Miltenyi Biotec; Bergisch Gladbach, Germany). After method optimization, it was identified that a minimum of 10,000 cells (25%) were necessary for accurate data (between 25% and 50% of the plated cells were analyzed per run for reported results). Data were analyzed using FlowJo software (Tree Star; Ashland, OR): briefly, the autogate function was used to identify the live cell population on a graph of forward scatter versus side scatter in order to reduce variability between experiments. The singlet live cell population was then separated from non-singlet live cells by a user-defined gate on a graph of forward scatter height versus forward scatter area. Finally, the data from a negative control consisting of uninfected A549 cells was gated on a fluorescence histogram graph to remove false GFP positives and split the live, singlet cell population into GFP-positive and GFP-negative. An example of the three gates applied to samples can be seen in the Supporting Information Figure S1. This gate was then applied to all other samples to identify the percentage of the population that was GFP-positive. The percentage of cells expressing GFP was compared against a standard curve using GraphPad Prism (GraphPad Software; La Jolla, CA) to generate a titre value. The

standard curve was generated using modality of infection (MOI) values ranging from 0.1 to 100 and can be found in the Supporting Information, Figure S2.

2.6. Calculation of characteristic shear rates

The nozzle operates with the excipient solution fed down a central channel by a peristaltic pump with the spray gas fed through a concentric channel around the liquid channel. The mixing zone occurs outside of the nozzle, as shown in Figure 1. External mixing nozzles allow for more control over atomization since both the liquid and spray gas flow rates can be controlled independently.²⁵

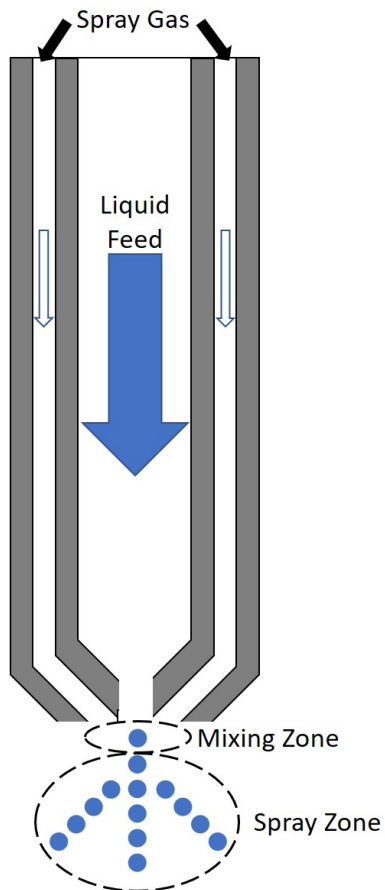


Figure 1: Schematic cross-section of a two-fluid external mixing nozzle such as the one used in this work.

The shear rate in the external mixing nozzle can be estimated as long as only the momentum transfer between the spray gas and liquid feed is considered. If the mass flow rate of liquid in the nozzle is similar to the mass flow rate of air in the nozzle, as is the case for our experiments using a lab-scale spray dryer, then the average velocity v_{av} (m/s) at the mixing point can be estimated by Equation 1:²⁵

$$v_{av} = \frac{v_{gas}}{1 + \frac{\dot{m}_{liq}}{\dot{m}_{gas}}} \quad (1)$$

where v_{gas} is the velocity of the spray gas at the point of atomization given in units of m/s, and \dot{m}_{liq} and \dot{m}_{gas} are the mass flow rates of the liquid feed and spray gas, respectively, in units of kg/s. For this calculation, the diameter of the inner nozzle tip was 0.7 mm, while the inner nozzle cap diameter was 1 mm and the outer nozzle cap diameter was 1.5 mm. The mass flow rates are calculated by converting the known volumetric flow rates in units of L/h using the density of either air (the spray gas) or the measured density of the excipient solution. A density of 1.225 kg/m³ was used for air and a density of 1060 kg/m³ was used as the average of the excipient solution samples. The average density was used to allow for direct comparisons between 4% and 8% solutions, causing a variation in the shear rate calculation of $\pm 3 \times 10^3 \text{ s}^{-1}$. Finally, an estimate for the characteristic shear rate $\dot{\gamma}$ in the spray dryer nozzle was made using Equation 2:^{9,25}

$$\dot{\gamma} = \frac{2(v_{av} - v_{liq})}{D_i} \quad (2)$$

where D_i is the inner diameter of the nozzle tip (0.7 mm) and v_{liq} is the velocity of the liquid at the point of atomization given in units of m/s.

2.6. Calculation of aggregate tensile strength

Equation 3 can be used to calculate the force necessary to break up particle aggregates:²⁶

$$\sigma = \frac{1.1 \left(\frac{1 - \varepsilon}{\varepsilon} \right) H}{d^2} \quad (3)$$

where σ is the tensile strength of the aggregate (N/m^2), ε is the void volume fraction of the aggregate (unitless), H is the force required to break the bond between individual particles [in Newtons], and d is the individual particle diameter [in meters]. In order to calculate the void volume fraction for each, Equation 4 can be used:

$$\varepsilon = \frac{4}{3} \pi \left(\frac{D}{2} \right)^2 - x \left(\frac{4}{3} \pi \left(\frac{d}{2} \right)^2 \right) \quad (4)$$

where D is the diameter of the aggregate given in m, and x is the number of individual particles that make up that aggregate (between two and four in this work).

2.7. Statistical analysis

All sheared samples were used to infect three wells of cells every time activity was evaluated, to assess the variability of the flow cytometry measurements. Quoted uncertainty in the measurements represented the standard deviation of triplicate well infections. Results were statistically analyzed using Microsoft Excel (Microsoft; Redmon, WA) and the Real Statistics Resource Pack plug-in, where applicable.²⁷ Viral activity results were considered statistically significantly different for $p \leq 0.05$ as determined using a one-way analysis of variance with a Tukey-Kramer Honestly Significant Difference (HSD) post hoc test. For aggregation tests, results were considered statistically significantly different for $p \leq 0.05$ as determined using a two-sided t-test.

It should be noted that characteristic shear rates of $97 \times 10^3 \text{ s}^{-1}$, $225 \times 10^3 \text{ s}^{-1}$, and $258 \times 10^3 \text{ s}^{-1}$ for the 4% formulation were tested separately from other shear rates due to a

defect in the stock viral vector suspension used, and that the shear rate of $433 \times 10^3 \text{ s}^{-1}$ has been omitted due to high variability in the activity (the standard deviation was greater than 60% of the mean, which should not be the case for flow cytometry data).

3. Results and Discussion

3.1. Effect of shear rate on viral vector activity

The viral vector AdHu5GFP in a 4% excipient solution of mannitol:dextran (3:1 weight ratio) was atomized through a spray dryer nozzle (without heat) at 15 different characteristic shear rates calculated using Equation 2, and listed in Table 1 along with the spray gas and liquid feed rate settings used for these experiments. Viral activity of the sheared fluid was reported as titre loss versus shear rate in Figure 2; throughout these discussions it was a matter of choice to reflect on viral efficacy based on ‘activity loss’ rather than ‘activity’. The spray gas rate, liquid feed rate and excipient concentration were selected based on previous spray drying experiments with the same viral vector.^{4,11} Figure 2 does not show the anticipated monotonic increase in viral titre loss with shear rate demonstrated previously in other works for bacteria but rather, at moderate shear conditions there was a decrease in activity loss.⁹ More specifically, the titre loss decreased from 3.72×10^6 pfu for the “zero shear” sample to a minimum value of 1.55×10^6 pfu ($p < 0.046$) at a shear rate of $391 \times 10^3 \text{ s}^{-1}$, above which the titre loss increased until it levelled off around 2.3×10^6 pfu at higher shear rates. Notably, all shear rates tested had lower activity losses than the “zero shear” sample, implying that shear (within the range tested) had an unexpectedly positive impact on viral activity.

Table 1. Characteristic shear rates in the spray dryer nozzle as determined by the spray dryer pump setting and the flow rate of the atomizing spray gas.

Liquid feed rate (mL/h) [Spray dryer pump setting (%)]
--

		188 [13]	290 [20]	440 [30]
Spray gas flow rate	282 [20]	$145 \times 10^3 \text{ s}^{-1}$	$121 \times 10^3 \text{ s}^{-1}$	$97 \times 10^3 \text{ s}^{-1}$
(L/h) [Spray dryer	439 [30]	$258 \times 10^3 \text{ s}^{-1}$	$225 \times 10^3 \text{ s}^{-1}$	$189 \times 10^3 \text{ s}^{-1}$
setting]	666 [40]	$433 \times 10^3 \text{ s}^{-1*}$	$391 \times 10^3 \text{ s}^{-1}$	$342 \times 10^3 \text{ s}^{-1}$
	1051 [50]	$736 \times 10^3 \text{ s}^{-1}$	$686 \times 10^3 \text{ s}^{-1}$	$623 \times 10^3 \text{ s}^{-1}$
	1373 [55]	$992 \times 10^3 \text{ s}^{-1}$	$938 \times 10^3 \text{ s}^{-1}$	$868 \times 10^3 \text{ s}^{-1}$

* The shear rate of $433 \times 10^3 \text{ s}^{-1}$ has been removed from activity results due to unusual variability.

Statistical analysis of data in Figure 2 showed that the titre loss at a shear rate of $391 \times 10^3 \text{ s}^{-1}$ was significantly different from the titer losses at 0, 97×10^3 , 121×10^3 , 225×10^3 , 258×10^3 , and $686 \times 10^3 \text{ s}^{-1}$ (indicated with asterisks over the plotted bars that were statistically different from the minimum which was itself denoted by a # in Figure 2). Statistical analysis increased our confidence in labelling this point a minimum, with at least one shear rate causing a statistically significant increase in titre losses on either side of $391 \times 10^3 \text{ s}^{-1}$. Each shear rate condition was repeated 3 to 4 times, and the *in vitro* activity testing was repeated in triplicate for each sample to assess the reproducibility of the methods; the precision is represented by the error bars in Figure 2 and is not identical for all data points but is small compared to the standard deviation values typically shown on log loss plots for activity loss after spray drying.^{4,11} Overall, small variability in the measured titre losses allow us to draw statistically relevant conclusions from the data set and recognize relevant fluctuations that suggest that there are optimal shear conditions that lead to smaller viral activity losses. This variability also accounts for the lack of pattern in the activity losses seen at the various non-significant shear rates, although the same statistically significant minima and overall trends appeared in repeated preliminary experiments (data not shown).

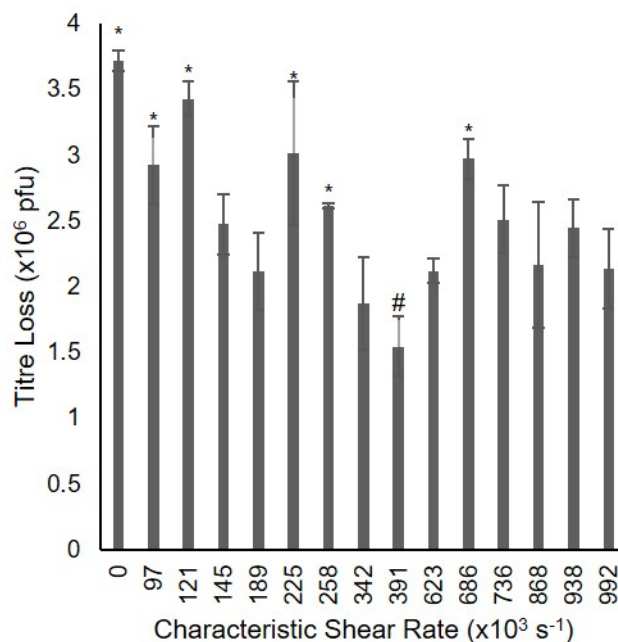


Figure 2: Titre loss of AdHu5GFP after shearing of a 4% mannitol/dextran and virus suspension at characteristic shear rates ranging from 97×10^3 to $992 \times 10^3 \text{ s}^{-1}$. Error bars represent standard deviation of triplicate infections from each shear rate. Data points marked with a (*) are statistically significantly different from the data point marked with a (#).

To support the phenomenon seen for AdHu5GFP in the 4% formulation, a more concentrated 8% excipient and virus suspension was subjected to the same range of discrete characteristic shear rates. Titre loss as a function of shear rate for the 8% samples is shown in Figure 3. Similar to the results with the 4% suspension, viral activity was improved at moderate shear rates compared to the “zero shear” sample. A significant minimum was seen at $258 \times 10^3 \text{ s}^{-1}$ ($p < 0.036$), which was lower than the shear rate that corresponded to the smallest activity loss for the 4% formulation. This minimum in titre loss ($1.73 \times 10^6 \text{ pfu}$) was statistically different from the losses at tested shear rates of 342×10^3 , 391×10^3 , 623×10^3 , 686×10^3 , 736×10^3 , and $938 \times 10^3 \text{ s}^{-1}$. With the more concentrated 8% suspension, two additional minima were

detected at $433 \times 10^3 \text{ s}^{-1}$ ($p < 0.044$) and $992 \times 10^3 \text{ s}^{-1}$ ($p < 0.050$), that could not be deemed statistically insignificant. While almost all titre loss values remained lower than the “zero shear” sample (except at $736 \times 10^3 \text{ s}^{-1}$) the activity losses were higher for 8% formulations compared to 4%.

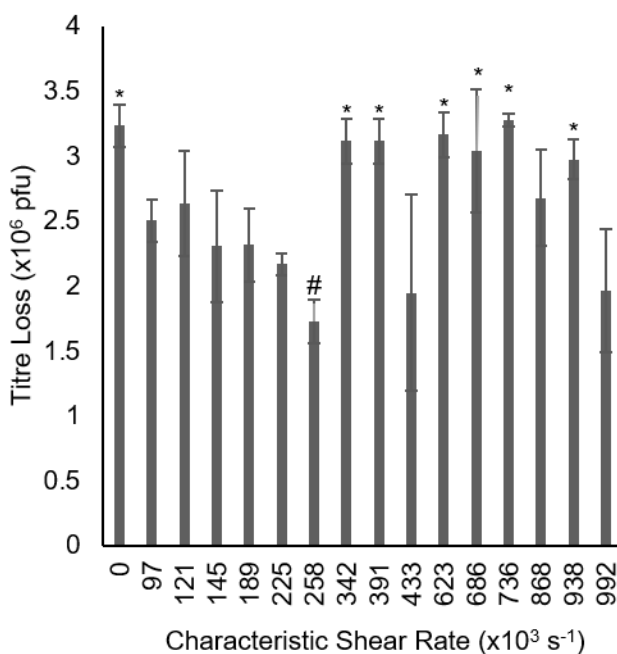


Figure 3: Titre loss of AdHu5GFP after shearing of an 8% mannitol/dextran and virus suspension at characteristic shear rates ranging from $97 \times 10^3 \text{ s}^{-1}$ to $992 \times 10^3 \text{ s}^{-1}$. Error bars represent standard deviation of triplicate infections from each shear rate. Data points marked with a (*) are statistically significantly different from the data point marked with a (#).

Importantly, the shear stresses applied in these experiments led to relatively small activity losses compared to normal spray drying losses, and under normal operating conditions, shear was deemed to not significantly impact viral efficacy. We note that the activity results in Figure 2 and Figure 3 are presented on a linear scale, not the more conventional *log* loss scale, to emphasize the differences between the various shear rates. If converted to log loss, the values for

the sheared 4% formulations ranged from 0.16 to 0.49 log and from 0.18 to 0.45 log for 8%, which are generally acceptable losses for manufacturing thermally stable vaccines. Compared to the losses expected in fully spray dried samples (with shear, atomization, heat and drying that are ca. 0.5 to 4 log loss) these values are small. Only in highly optimized systems have we achieved losses of less than 0.5 log after spray drying with this formulation.¹⁰ As such, even at the highest shear rates tested, viral activity was relatively well-maintained in this study.

From the fluctuations in titre loss measured over the large range of shear rates (and shear stresses) we infer that several physical mechanisms were affecting viral activity. We hypothesized that viral aggregates were present in the “zero shear” and lower shear rate samples, causing the increased activity loss due to a decrease in free non-aggregated viruses available to infect cells. If this aggregation is produced by diluting viral vectors in solutions of mixed saccharides, it would be a new concern for the field of thermally stable vaccines. Following this hypothesis, the single minimum in viral activity loss measured with the 4% suspension and the three minima associated with the 8% suspension were assumed to be caused by the break up of different aggregates once a critical shear stress was applied, where the specific critical shear stress was related to the size of the aggregate.

Superimposed on this aggregation phenomenon, increasing shear stresses had a detrimental effect on the structural integrity of the viral vector, albeit minor, causing activity losses to increase after the minima, though only up to a plateau in titre loss. It is reasonable to believe that this damage occurs in the mixing zone of the nozzle where shear stresses are magnitudes higher than before or afterwards in the process (Figure 1). Adenoviruses, such as AdHu5GFP used here, are composed of a non-enveloped icosahedral capsid containing genetic information, with elongated fiber-like proteins extending from each of the 12 vertices of the

capsid.²⁸ These fibers are responsible for binding to cellular receptors for initiation of the infection process, however are considered very fragile and are the most probable candidates for shear damage in the virus structure.²⁹ The next section examines the hypothesis of viral aggregation and the effects of shear on de-aggregation.

3.2 Effect of shear rate on viral vector aggregation

Viral particle size was measured using the qViro-X technique for control samples and samples that had been subjected to shear rates of 0, 121×10^3 , 391×10^3 , and $686 \times 10^3 \text{ s}^{-1}$ for 4% formulations, and 0, 121×10^3 , 258×10^3 , and $686 \times 10^3 \text{ s}^{-1}$ for 8% formulations. These samples were chosen so that there would be aggregation data from zero shear up to shear rates encompassing one activity loss minima for each formulation. The cut-off particle size for the measurements was set at 420 nm by the nanopore size of the qViro-X membrane used. Figure 4(a) shows the particle size distributions for the controls: (1) a viral vector stock suspension and (2) a UV-deactivated sample of the same viral vector stock suspension – neither sample included excipients nor were they sheared. The distributions are overlaid to highlight the difference between an unaggregated and highly aggregated sample. UV deactivation of adenoviruses has been shown to primarily occur due to viral DNA damage; aggregation of the deactivated sample is a likely side effect of the deactivation process caused by adenoviral protein damage.^{30,31}

The control stock suspension was found to contain particles with a monomodal size distribution, including few aggregates (with sizes larger than 129 nm), giving a mean particle diameter of $99 \pm 17 \text{ nm}$. This is consistent with the range of 70 – 100 nm cited in the literature for primary adenovirus particles, as well as values measured by the same technique.^{32,33} Defining 129 nm as the “cut-off” above which particles are considered aggregated is explained below with Table 2. The near-absence of aggregates in the stock suspension matches with previous findings

using disc centrifugation.³⁴ The size distribution of the other control, the UV-deactivated sample, had a similar monomodal distribution with a broader right-sided shoulder (with a mean of 113 ± 28 nm) and had many more particles larger than 129 nm, i.e., aggregates, than present in the stock suspension. These results were primarily used to validate the use of the qViro-X technique to measure adenoviral aggregation. Figure 4(b) and 4(c) show the size distribution of the 4% and 8% formulation “zero shear” samples for comparison. The distributions more closely resemble the stock viral suspension than the UV-deactivated sample, but include more aggregates than the former case. The size distributions for the other six samples can be found in the Supporting Information, Figures S3 – S8.


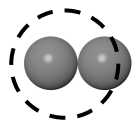
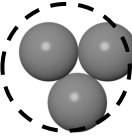
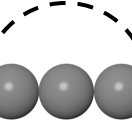
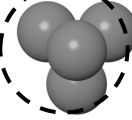


Figure 4: (a) Comparison of the size distributions for the stock adenovirus control (particle count of 933) and a UV-deactivated virus control (particle count of 218). The stock sample has a main peak of single virus particles with a few larger aggregates; the deactivated sample has a main peak that is centered around a larger diameter, has a large right-sided shoulder, and many more large aggregates. (b) Size distribution of the 4% formulation “zero shear” sample (particle count of 488). (c) Size distribution of the 8% formulation “zero shear” sample (particle count of 406).

To understand the de-aggregation mechanics and assess whether the changes in number/size of aggregates could explain the decrease in titer loss at certain shear rates during atomization, the possible geometric make-up of viral aggregates first needed to be estimated. The icosahedral shape of the adenovirus can be well approximated by a sphere.³⁵ Based on this assumption, a radius of gyration (R) could be assigned to aggregates composed of two, three, and four primary viral particles (with radius R_0) following the work of McEvoy et al., who predicted the size of influenza virus aggregates.³⁶ Aggregate geometry allows the calculation of the void volume fraction, which in turn may be used to estimate the bond strength between cohesively attached particles. Although changes in the geometry of an individual viral particle would affect the void volume, studies on the mechanical strength of adenovirus capsids suggests that forces higher than those used in this study are necessary for deformation.^{16,37} The various aggregates, equations, and calculated diameters were derived using a primary particle diameter of 99 nm and are summarized in Table 2, along with the estimated void volume fraction for each aggregate (Equation 4). It should be noted that these geometries are intended only as an estimate in order to interpret aggregation results, and that the actual aggregates will vary somewhat due to the variability of size and shape naturally present in the viral particles. The volume-based diameters calculated in Table 2 for suggested available geometries are compared to measured aggregates above 129 nm in Figure 5 for both the 4% and 8% formulation samples; the diameter of 129 nm was selected as the “cut-off” by taking the smallest measured adenovirus diameter (72 nm) and using the dimer formula in Table 2 to calculate the smallest potential aggregate size. Since a primary viral particle may vary between 72-105 nm (Figure 4), the calculated sizes shown in the figure are merely representative of a geometry, we do not believe that the geometries used in this

analysis describe all possible aggregate geometries present in the suspension. It was simply needed that the measured aggregates and predicted geometries were similar in size in order to later estimate the tensile strength of these aggregates.

Table 2: Equations and calculated volume-based diameters to estimate the size of four different configurations of adenovirus aggregates, as well as void volume fractions (for calculating adenovirus bond strength) calculated using Equation 4. The dotted circles denote the hydrodynamic volumes represented by these geometries.

Aggregate Geometry	Equation*	Calculated Diameter (nm)	Void Volume Fraction
 Monomer	$R = R_0$	99	-
 Dimer	$R^2 = \frac{16}{5} R_0^2$	177	0.65
 Triangular trimer	$R^2 = \frac{29}{5} R_0^2$	238	0.78
 Linear trimer	$R^2 = \frac{49}{5} R_0^2$	310	0.90
 Pyramidal tetramer	$R^2 = \frac{37}{5} R_0^2$	270	0.80

* from ³⁶

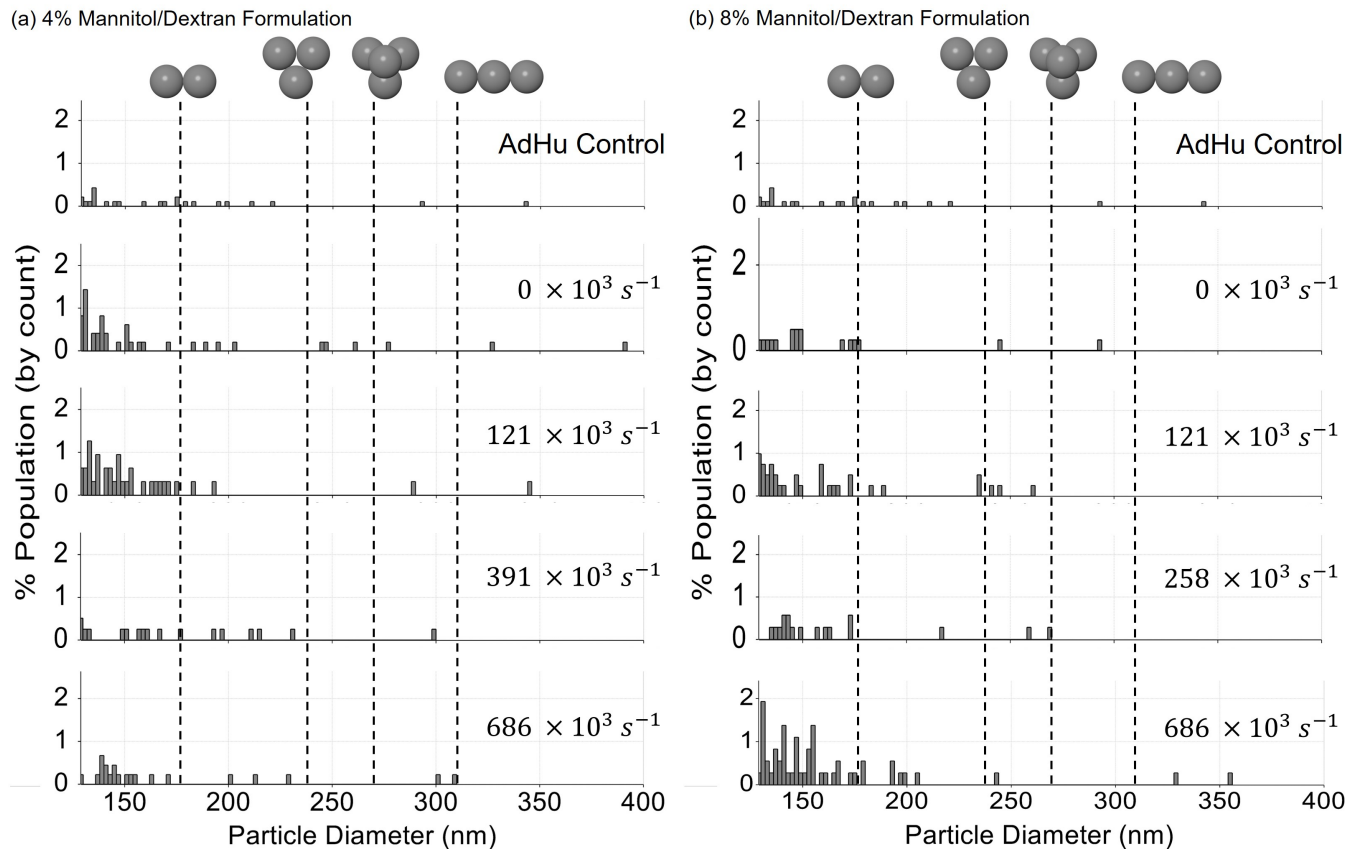


Figure 5: Comparison of predicted aggregate diameters with measured adenovirus particle diameters above 129 nm for (a) 4% formulations with no applied shear (“zero shear” sample), an applied shear rate of 121×10^3 , 391×10^3 , and 686×10^3 s^{-1} (from top to bottom); and (b) 8% formulations with no applied shear (“zero shear” sample), an applied shear rate of 121×10^3 , 258×10^3 , and 686×10^3 s^{-1} (from top to bottom).

For trials with the 4% formulation, the “zero shear” sample had the highest frequency of large aggregates relative to the stock suspension among the sheared samples, as seen in Figure 5(a). These aggregates were a result of the stock suspension being added to the solution with excipients. Observed aggregates were largely dimers yet included larger masses consisting of at least three to four adenoviruses like the pyramidal tetramer or linear trimer. As the shear rate was

increased from 0, the largest aggregates (close to 400 nm) no longer appeared in the analysis, possibly fractured since they would be the weakest of the particles shown in the figure; at each shear rate, only a critical aggregate size will persist whereas larger particles will break apart according to Rumpf's theory for the fracture strength of agglomerated solids.²⁶ After shearing at $121 \times 10^3 \text{ s}^{-1}$, newer particle sizes around 340 nm appear that may be related to fracturing of those larger aggregates or simply other geometric configurations not capable of being broken up at this shear rate. At a shear rate of $391 \times 10^3 \text{ s}^{-1}$, the particle size distribution most closely resembled the control stock viral suspension supporting that the minimum in activity loss at this shear rate for the 4% formulation is linked to the state of viral aggregation.

However, when the shear rate was increased further to $686 \times 10^3 \text{ s}^{-1}$, the amount of dimer aggregates present in the 4% formulation increased relative to the sample collected at $391 \times 10^3 \text{ s}^{-1}$ though the maximum aggregate size remained similar; both the $391 \times 10^3 \text{ s}^{-1}$ and the $686 \times 10^3 \text{ s}^{-1}$ shear rates had aggregate sizes that suggested both the triangular and linear trimers, but not the pyramidal tetramer. The production of new (but relatively small) aggregates at $686 \times 10^3 \text{ s}^{-1}$ is thought to be due to removal of the fiber-like proteins on the viral capsid under these shear forces, allowing for stronger cohesive bridging between viral particles. Although the shoulder on the distribution at approximately 125 nm is at a diameter smaller than that predicted in Table 2 for dimer aggregates, it is thought to be composed of dimers of viral particles with primary diameters smaller than 99 nm, or dimers of shear-damaged viral particles without fiber proteins, causing them to appear smaller than predicted.

For trials with the 8% formulation, all sheared samples and the 'zero shear' sample showed more aggregation than the control stock suspension, as seen in Figure 5(b). Though difficult to make definitive conclusions from the data, it did not appear that there were more or

larger aggregates at this higher excipient concentration in the ‘zero shear’ sample. This indicates that the concentration of the excipients at 4% was sufficient to affect the virus population in suspension and the higher concentration produced no new interactions that would lead to further aggregation. As observed with the 4% formulation, the largest aggregate size decreased in samples by increasing shear from 0 to $121 \times 10^3 \text{ s}^{-1}$ while the amount of overall aggregation remained similar between the two operating states. The sample sheared at $258 \times 10^3 \text{ s}^{-1}$ (the first minimum in Figure 3) showed the least amount of total aggregation, and had a similar maximum aggregate size to the $121 \times 10^3 \text{ s}^{-1}$ sheared sample; the particle size distribution was not as close to the control stock suspension as seen for the 4% formulation at the shear rate corresponding to minimum activity loss but the sample did contain considerably fewer aggregates than at other shear condition. The sample subjected to $686 \times 10^3 \text{ s}^{-1}$ displayed the most aggregates as well as the largest aggregates for the 8% formulation. Based on the higher shear stresses afforded by its higher suspension viscosity, a higher frequency of viruses in this sample were expected to experience damaged capsid fibers, giving the greatest degree of aggregation and deactivation observed.

With only two formulation concentrations studied, we cannot fully model the trend between concentration and the shear rate at which titre loss minima are seen, however, the two-fold increase in concentration from 4% to 8% caused a 1.5-fold decrease in the shear rate that minimized activity loss, suggesting an inverse linear relationship between concentration and minimal shear rate. As the concentration, and therefore viscosity, of the suspension increases, it is more likely that damage to the viral structure, and further aggregation, will occur at high shear rates. Therefore, it is recommended to err on the lower end of the applied shear rates during processing, particularly when using more concentrated excipient formulations.

Comparing the particle size distributions in Figure 5 to the titre loss data in Figures 2 and 3, the degree to which viruses were bound in aggregates correlated with higher activity losses. At low or zero shear conditions, the occurring aggregation was attributed to the stock virus suspension being mixed with the excipient saccharides. The mean particle diameters (Supporting Information Table S1) support this finding, showing the samples from both 4% and 8% formulations at “zero shear” had mean particle diameters (104 ± 27 and 103 ± 18 nm, respectively) that were statistically higher than that of the viral stock suspension (99 ± 17 nm) ($p < 0.05$). From this we infer that excipient concentration does not appear to significantly affect aggregation and although the cause of ‘aggregation due to mixing’ is unknown, changes in local ionic strength or pH as the virus and mixed saccharides are brought together may be contributing factors.³⁸ For both 4% and 8% formulations, the samples showing the least aggregation in Figure 5 ($391 \times 10^3 \text{ s}^{-1}$ and $258 \times 10^3 \text{ s}^{-1}$, respectively) correspond to an activity loss minima; the lower shear rate for the minima in the 8% suspension can be attributed to its higher viscosity, indicating the phenomenon was shear stress dependent which would be consistent with an aggregate’s fracture strength. Motion through the velocity gradients in the nozzle and mixing zone as the liquid formulation is compressed can increase particle-particle collisions leading to further aggregation and therefore differing aggregate sizes in the sheared samples.^{39,40} The detailed fluid dynamics of the spray dryer nozzle and mixing zone are outside the scope of this work; however, Hede et al. noted that turbulent flow is necessary to break up the liquid flow into droplets.²⁵ The secondary mechanism for aggregation was attributed to damaged capsid fibers that occurred at higher shear rates. Removal of the viral capsid fiber proteins would allow for closer packing of virus particles, leading to new interparticle bonds and therefore aggregates to

be created. These damage-induced aggregates may contribute to the second and third activity minima seen in the 8% formulation as they are broken up.

3.3. Strength of a viral aggregate

Accepting the proposed aggregate geometries above, and the evidence that the minima for titer loss seen with the 4% and 8% formulations corresponded to one or more of these aggregate geometries breaking up, it is possible to estimate the (tensile) fracture strength of these aggregates based on the corresponding shear stress when break up occurred. Equation 3 can be rearranged to calculate H , the interparticle bond strength between two adenovirus particles, giving researchers a valuable parameter for predicting process conditions that favor de-aggregation. To the best of our knowledge, this H value has not been reported in the literature previously for adenoviruses. The estimated value will be limited to adenoviral suspensions of comparable viscosity to our formulations, namely $1.1 \times 10^{-3} \text{ Pa} \cdot \text{s}$ and $1.3 \times 10^{-3} \text{ Pa} \cdot \text{s}$, for 4% and 8%, respectively, and displaying Newtonian behaviour across the range of shear conditions under consideration. This Newtonian behaviour, as expected for aqueous dextran solutions, means that there will be a linear relationship between the shear rate and the shear stress in the nozzle.⁴¹ The shear rates at activity loss minima were equated to the break up of aggregate sizes based on their calculated void volume fractions, with the highest void volume fraction aggregate being considered to fracture at the lowest shear rate minima and the lowest void volume fraction aggregate fracturing at the highest shear rate minima per formulation.

Table 3 gives the tensile fracture strengths of each aggregate, ordered from lowest to highest in terms of volume fraction, calculated using the given suspension viscosities and shear rates. The calculated values for the viral interparticle bond strength are all of similar magnitude, between 10 and 33 pN, leading us to conclude that the assumptions above were reasonable.

These calculated H values are similar to those reported by Dobrowsky et al. for the strength of adhesion between HIV surface proteins and cellular receptors, which ranged between 18 and 33 pN.⁴² The difference in calculated bond strength for the linear trimer in the 4% and 8% formulations is small and within the error of the calculation based on the error in shear rate calculations. As a result of this analysis, we conclude that 25 pN is a reasonable estimate of the viral bond strength, which should allow researchers to predict the shear rates that correspond to activity loss minima based on the viscosity of their suspensions being spray dried.

Table 3: The tensile strength required to break up each viral aggregate geometry at the various activity loss minima in the 4% and 8% formulations. The tensile strength values were then used to calculate the viral interparticle bond strengths with Equation 3.

Aggregate Geometry (Concentration used in Calculation)	Shear rate @ minima ($\times 10^3 \text{s}^{-1}$)	Tensile strength (N/m^2)	Bond strength (pN)
Linear trimer (8%)	258	347	28
Linear trimer (4%)	391	417	33
Pyramidal tetramer (8%)	433	583	21
Triangular trimer (8%)	433	583	18
Dimer (8%)	992	1335	10

4. Conclusion

Overall, these data show that there are several mechanisms acting on the virus during the atomization step of thermally stable dry powder vaccine production, impacting both viral activity and aggregation. Initial mild aggregation occurs when the stock adenovirus suspension is mixed with excipients, and similarly increased aggregation is seen at higher shear rates caused by damage to the viral capsid fibers, along with increased activity losses. Some of the initial minor

aggregation can be reversed by applying moderate shear stresses to the sample, leading to minima in measured activity losses. The exact shear rate at which the most de-aggregation and activity recovery occurs, varies depending on the formulation viscosity, with higher viscosity suspensions requiring a lower shear rate to minimize activity loss. While the highest shear rates used in this work caused damage to the viral capsid fibers and an increase in activity loss, the overall effect of shear on adenovirus activity is low compared to conventional spray drying losses and in line with other findings in the literature that shear has little to no effect on the biologic and even at the highest shear rate, viral activity was maintained. If optimization during formulation development is possible, the spray gas and liquid feed rates can be tuned based on suspension viscosity and viral aggregate tensile strength to minimize viral vector activity loss.

Supporting Information

Example for the live cell population, singlet cell population, and GFP positive/negative population gates applied to flow cytometry samples; the standard curve used to analyze flow cytometry data; particle size distributions for the seven samples not shown in main text; table of mean and mode particle diameters for both 4% and 8% formulations.

Acknowledgements

The authors thank Prof. K. Mossman for equipment use; Sam Afkhami, Xueya Feng and Anna Zganiacz for cell culture training and assistance; and Susan Collins, Heera Marway and Zoya Tabunshchyk for equipment training and troubleshooting help. This study is supported by funds from the Canadian Institutes of Health Research, the Natural Sciences and Engineering Research Council of Canada, and Ontario Centres of Excellence (OCE) (Collaborative Health Research Program CHRP523837-18).

References

- (1) Ohtake, S.; Martin, R. A.; Yee, L.; Chen, D.; Kristensen, D. D.; Lechuga-Ballesteros, D.; Truong-Le, V. Heat-Stable Measles Vaccine Produced by Spray Drying. *Vaccine* **2010**, *28* (5), 1275–1284. <https://doi.org/10.1016/j.vaccine.2009.11.024>.
- (2) Corbanie, E. A.; Remon, J. P.; Reeth, K. Van; Landman, W. J. M.; Eck, J. H. H. Van; Vervaet, C. Spray Drying of an Attenuated Live Newcastle Disease Vaccine Virus Intended for Respiratory Mass Vaccination of Poultry. *Vaccine* **2007**, *25*, 8306–8317. <https://doi.org/10.1016/j.vaccine.2007.09.049>.
- (3) LeClair, D. A.; Li, L.; Rahman, N.; Cranston, E. D.; Thompson, M. R. Stabilization of HSV-2 Viral Vaccine Candidate by Spray Drying. *Int. J. Pharm.* **2019**, *569* (May), 118615. <https://doi.org/10.1016/j.ijpharm.2019.118615>.
- (4) LeClair, D. A.; Cranston, E. D.; Xing, Z.; Thompson, M. R. Evaluation of Excipients for Enhanced Thermal Stabilization of a Human Type 5 Adenoviral Vector through Spray Drying. *Int. J. Pharm.* **2016**, *506* (1–2), 289–301. <https://doi.org/10.1016/j.ijpharm.2016.04.067>.
- (5) Grasmeijer, N. Improving Protein Stabilization by Spray Drying: Formulation and Process Development, University of Groningen, 2016.
- (6) Saluja, V.; Amorij, J.-P.; Kapteyn, J. C.; de Boer, A. H.; Frijlink, H. W.; Hinrichs, W. L. J. A Comparison between Spray Drying and Spray Freeze Drying to Produce an Influenza Subunit Vaccine Powder for Inhalation. *J. Controlled Release* **2010**, *144* (2), 127–133. <https://doi.org/10.1016/j.jconrel.2010.02.025>.
- (7) Maa, Y.-F.; Hsu, C. C. Effect of High Shear on Proteins. *Biotechnol. Bioeng.* **1996**, *51* (4), 458–465. [https://doi.org/10.1002/\(SICI\)1097-0290\(19960820\)51:4<458::AID-BIT9>3.0.CO;2-H](https://doi.org/10.1002/(SICI)1097-0290(19960820)51:4<458::AID-BIT9>3.0.CO;2-H).

- (8) Perdana, J.; Fox, M. B.; Schutyser, M. A. I.; Boom, R. M. Enzyme Inactivation Kinetics: Coupled Effects of Temperature and Moisture Content. *Food Chem.* **2012**, *133* (1), 116–123. <https://doi.org/10.1016/j.foodchem.2011.12.080>.
- (9) Ghandi, A.; Powell, I. B.; Howes, T.; Chen, X. D.; Adhikari, B. Effect of Shear Rate and Oxygen Stresses on the Survival of *Lactococcus Lactis* during the Atomization and Drying Stages of Spray Drying: A Laboratory and Pilot Scale Study. *J. Food Eng.* **2012**, *113* (2), 194–200. <https://doi.org/10.1016/j.jfoodeng.2012.06.005>.
- (10) LeClair, D. A.; Cranston, E. D.; Xing, Z.; Thompson, M. R. Optimization of Spray Drying Conditions for Yield, Particle Size and Biological Activity of Thermally Stable Viral Vectors. *Pharm. Res.* **2016**, *33* (11), 2763–2776. <https://doi.org/10.1007/s11095-016-2003-4>.
- (11) Morgan, B. A.; Xing, Z.; Cranston, E. D.; Thompson, M. R. Acoustic Levitation as a Screening Method for Excipient Selection in the Development of Dry Powder Vaccines. *Int. J. Pharm.* **2019**, *563* (March), 71–78. <https://doi.org/10.1016/j.ijpharm.2019.03.026>.
- (12) He, P.; Davis, S. S.; Illum, L. Chitosan Microspheres Prepared by Spray Drying. *Int. J. Pharm.* **1999**, *187* (1), 53–65. [https://doi.org/10.1016/S0378-5173\(99\)00125-8](https://doi.org/10.1016/S0378-5173(99)00125-8).
- (13) Gong, P.; Zhang, L.; Han, X.; Shigwedha, N.; Song, W.; Yi, H.; Du, M.; Cao, C. Injury Mechanisms of Lactic Acid Bacteria Starter Cultures During Spray Drying : A Review. *Drying Technol.* **2014**, *32*, 793–800. <https://doi.org/10.1080/07373937.2013.860458>.
- (14) To, B. C. S.; Etzel, M. R. Survival of *Brevibacterium Linens* (ATCC 9174) after Spray Drying , Freeze Drying , or Freezing. *J. Food Sci.* **1997**, *62* (1), 167–170. <https://doi.org/https://doi.org/10.1111/j.1365-2621.1997.tb04392.x>.
- (15) Shiu, C.; Zhang, Z.; Thomas, C. A Comparison of the Mechanical Properties of Different

- Bacterial Species. In *Focus on Biotechnology*, vol. 2; Springer, Dordrecht, 2001; pp 155–162. https://doi.org/10.1007/0-306-46888-3_11.
- (16) Snijder, J.; Reddy, V. S.; May, E. R.; Roos, W. H.; Nemerow, G. R.; Wuite, G. J. L. Integrin and Defensin Modulate the Mechanical Properties of Adenovirus. *J. Virol.* **2013**, *87* (5), 2756–2766. <https://doi.org/10.1128/jvi.02516-12>.
- (17) Levy, M. S.; Collins, I. J.; Yim, S. S.; Ward, J. M.; Shamlou, P. A.; Dunnill, P. Effect of Shear on Plasmid DNA in Solution. *Bioprocess Eng.* **1999**, *20*, 7–13. <https://doi.org/https://doi.org/10.1007/s004490050552>.
- (18) Maa, Y. F.; Hsu, C. C. Protein Denaturation by Combined Effect of Shear and Air-Liquid Interface. *Biotechnol. Bioeng.* **1997**, *54* (6), 503–512. [https://doi.org/10.1002/\(SICI\)1097-0290\(19970620\)54:6<503::AID-BIT1>3.0.CO;2-N](https://doi.org/10.1002/(SICI)1097-0290(19970620)54:6<503::AID-BIT1>3.0.CO;2-N).
- (19) Michalsky, R.; Pfromm, P. H.; Czermak, P.; Sorensen, C. M.; Passarelli, A. L. Effects of Temperature and Shear Force on Infectivity of the Baculovirus Autographa Californica M Nucleopolyhedrovirus. *J. Virol. Methods* **2008**, *153*, 90–96. <https://doi.org/10.1016/j.jviromet.2008.07.030>.
- (20) D’Souza, D. H.; Su, X.; Roach, A.; Harte, F. High-Pressure Homogenization for the Inactivation of Human Enteric Virus Surrogates. *J. Food Prot.* **2009**, *72* (11), 2418–2422. <https://doi.org/10.4315/0362-028x-72.11.2418>.
- (21) Wang, J.; Thorson, L.; Stokes, R. W.; Santosuosso, M.; Huygen, K.; Zganiacz, A.; Hitt, M.; Xing, Z. Single Mucosal, but Not Parenteral, Immunization with Recombinant Adenoviral-Based Vaccine Provides Potent Protection from Pulmonary Tuberculosis. *J. Immunol.* **2004**, *173* (10), 6357–6365. <https://doi.org/10.4049/jimmunol.173.10.6357>.
- (22) Roediger, E. K.; Kugathasan, K.; Zhang, X. Z.; Lichty, B. D.; Xing, Z. Heterologous

- Boosting of Recombinant Adenoviral Prime Immunization with a Novel Vesicular Stomatitis Virus-Vectored Tuberculosis Vaccine. *Mol. Ther.* **2008**, *16* (6), 1161–1169. <https://doi.org/10.1038/mt.2008.59>.
- (23) Toniolo, S. P.; Afkhami, S.; Mahmood, A.; Fradin, C.; Lichty, B. D.; Miller, M. S.; Xing, Z.; Cranston, E. D.; Thompson, M. R. Excipient Selection for Thermally Stable Enveloped and Non-Enveloped Viral Vaccine Platforms in Dry Powders. *Int. J. Pharm.* **2019**, *561* (January), 66–73. <https://doi.org/10.1016/j.ijpharm.2019.02.035>.
- (24) Thompson, M. R.; Xing, Z.; LeClair, D. A.; Cranston, E. D. Enhanced Thermal Stability for Adenoviral Vectors through Spray Drying. US20190062692A1, 2019.
- (25) Hede, P. D.; Bach, P.; Jensen, A. D. Two-Fluid Spray Atomisation and Pneumatic Nozzles for Fluid Bed Coating / Agglomeration Purposes : A Review. *Chem. Eng. Sci.* **2008**, *63*, 3821–3842. <https://doi.org/10.1016/j.ces.2008.04.014>.
- (26) Rumpf, H. The Strength of Granules and Agglomerates. *Agglom. First Int. Symp. Agglom. Philadelphia, 1962* **1962**, 379–418.
- (27) Zaiontz, C. Real Statistics Resource Pack (Release 6.2). 2019.
- (28) Appaiahgari, M. B.; Vrati, S. Adenoviruses as Gene/Vaccine Delivery Vectors: Promises and Pitfalls. *Expert Opin. Biol. Ther.* **2015**, *15* (3), 337–351. <https://doi.org/10.1517/14712598.2015.993374>.
- (29) Lasaro, M. O.; Ertl, H. C. J. New Insights on Adenovirus as Vaccine Vectors. *Mol. Ther.* **2009**, *17* (8), 1333–1339. <https://doi.org/10.1038/mt.2009.130>.
- (30) Eischeid, A. C.; Meyer, J. N.; Linden, K. G. UV Disinfection of Adenoviruses: Molecular Indications of DNA Damage Efficiency. *Appl. Environ. Microbiol.* **2009**, *75* (1), 23–28. <https://doi.org/10.1128/AEM.02199-08>.

- (31) Beck, S. E.; Hull, N. M.; Poepping, C.; Linden, K. G. Wavelength-Dependent Damage to Adenoviral Proteins across the Germicidal UV Spectrum. *Environ. Sci. Technol.* **2018**, *52* (1), 223–229. <https://doi.org/10.1021/acs.est.7b04602>.
- (32) Vogel, R.; Willmott, G.; Kozak, D.; Roberts, G. S.; Anderson, W.; Groenewegen, L.; Glossop, B.; Barnett, A.; Turner, A.; Trau, M. Quantitative Sizing of Nano/Microparticles with a Tunable Elastomeric Pore Sensor. *Anal. Chem.* **2011**, *83*, 3499–3506. <https://doi.org/10.1021/ac200195n>.
- (33) Kennedy, M. A.; Parks, R. J. Adenovirus Virion Stability and the Viral Genome: Size Matters. *Mol. Ther.* **2009**, *17* (10), 1664–1666. <https://doi.org/10.1038/mt.2009.202>.
- (34) Bondoc Jr., L. L.; Fitzpatrick, S. Size Distribution Analysis of Recombinant Adenovirus Using Disc Centrifugation. *J. Ind. Microbiol. Biotechnol.* **1998**, *20*, 317–322. <https://doi.org/10.1038/sj.jim.2900529>.
- (35) Berkowitz, S. A.; Philo, J. S. Monitoring the Homogeneity of Adenovirus Preparations (a Gene Therapy Delivery System) Using Analytical Ultracentrifugation. *Anal. Biochem.* **2007**, *362*, 16–37. <https://doi.org/10.1016/j.ab.2006.11.031>.
- (36) McEvoy, M.; Razinkov, V.; Wei, Z.; Casas-Finet, J. R.; Tous, G. I.; Schenerman, M. A. Improved Particle Counting and Size Distribution Determination of Aggregated Virus Populations by Asymmetric Flow Field-Flow Fractionation and Multiangle Light Scattering Techniques. *Biotechnol. Prog.* **2011**, *27* (2), 547–554. <https://doi.org/10.1002/btpr.499>.
- (37) Ortega-Esteban, A.; Horcas, I.; Hernando-Pérez, M.; Ares, P.; Pérez-Berná, A. J.; San Martín, C.; Carrascosa, J. L.; De Pablo, P. J.; Gómez-Herrero, J. Minimizing Tip-Sample Forces in Jumping Mode Atomic Force Microscopy in Liquid. *Ultramicroscopy* **2012**, *114*,

- 56–61. <https://doi.org/10.1016/j.ultramic.2012.01.007>.
- (38) Rexroad, J.; Evans, R. K.; Middaugh, C. R. Effect of PH and Ionic Strength on the Physical Stability of Adenovirus Type 5. *J. Pharm. Sci.* **2006**, *95* (2), 237–247. <https://doi.org/10.1002/jps.20496>.
- (39) Flesch, J. C.; Spicer, P. T.; Pratsinis, S. E. Laminar and Turbulent Shear-Induced Flocculation of Fractal Aggregates. *AIChE J.* **1999**, *45* (5), 1114–1124. <https://doi.org/10.1002/aic.690450518>.
- (40) Meakin, P. Fractal Aggregates. *Adv. Colloid Interface Sci.* **1987**, *28*, 249–331. [https://doi.org/10.1016/0001-8686\(87\)80016-7](https://doi.org/10.1016/0001-8686(87)80016-7).
- (41) Carrasco, F.; Chornet, E.; Overend, R. P.; Costa, J. A Generalized Correlation for the Viscosity of Dextrans in Aqueous Solutions as a Function of Temperature, Concentration, and Molecular Weight at Low Shear Rates. *J. Appl. Polym. Sci.* **1989**, *37* (8), 2087–2098. <https://doi.org/10.1002/app.1989.070370801>.
- (42) Dobrowsky, T. M.; Rabi, S. A.; Nedellec, R.; Daniels, B. R.; Mullins, J. I.; Mosier, D. E.; Siliciano, R. F.; Wirtz, D. Adhesion and Fusion Efficiencies of Human Immunodeficiency Virus Type 1 (HIV-1) Surface Proteins. *Sci. Rep.* **2013**, *3*, 1–9. <https://doi.org/10.1038/srep03014>.